Imaging Science in Dentistry 2023; 53: 127-35
https://doi.org/10.5624/isd.20220185

The effects of different metal posts, cements, and exposure parameters on cone-beam computed tomography artifacts

Ana Priscila Lira de Farias Freitas[1], Larissa Rangel Peixoto[1], Fernanda Clotilde Mariz Suassuna[1], Patrícia Meira Bento[1], Ana Marly Araújo Maia Amorim[1], Karla Rovaris Silva[2], Renata Quirino de Almeida Barros[3], Andrea dos Anjos Pontual de Andrade Lima[4], Daniela Pita de Melo[1,*]

[1]*Department of Oral Diagnosis, State University of Paraíba, Campina Grande, PB, Brazil*
[2]*Department of Oral Diagnosis, Federal University of Piauí, Teresina, PI, Brazil*
[3]*Departmentof Oral Imaging of Unifacisa, Campina Grande, PB, Brazil*
[4]*Department of Oral Diagnosis, Federal University of Pernambuco, Campina Grande, PB, Brazil*

ABSTRACT

Purpose: This study assessed the intensity of artifacts produced by 2 metal posts, 2 cements, and different exposure parameters using 2 cone-beam computed tomography (CBCT) units.

Materials and Methods: The sample was composed of 20 single-rooted premolars, divided into 4 groups: Ni-Cr/zinc phosphate, Ni-Cr/resin cement, Ag-Pd/zinc phosphate, and Ag-Pd/resin cement. Samples were scanned before and after post insertion and cementation using a CS9000 3D scanner with 4 exposure parameters (85/90 kV and 6.3/10 mA) and an i-CAT scanner with 120 kV and 5 mA. The presence of artifacts was assessed subjectively by 2 observers and objectively by a trained observer using ImageJ software. The Mann-Whitney, Wilcoxon, weighted kappa, and chi-square tests were used to assess data at a 95% confidence level ($\alpha < 0.05$).

Results: In the subjective analyses, AgPd presented more hypodense and hyperdense lines than NiCr ($P < 0.05$), and more hypodense halos were found using i-CAT ($P < 0.05$) than using CS9000 3D. More hypodense halos, hypodense lines, and hyperdense lines were observed at 10 mA than at 6.3 mA ($P < 0.05$). More hypodense halos were observed at 85 kV than at 90 kV ($P < 0.05$). CS9000 3D presented more hypodense and hyperdense lines than i-CAT ($P < 0.05$). In the objective analyses, AgPd presented higher percentages of hyperdense and hypodense artifacts than NiCr ($P < 0.05$). Zinc phosphate cement presented higher hyperdense artifact percentages on CS9000 3D scans ($P < 0.05$). CS9000 3D presented higher artifact percentages than i-CAT ($P < 0.05$).

Conclusion: High-atomic-number alloys, higher tube current, and lower tube voltage may increase the artifacts present in CBCT images. ***(Imaging Sci Dent 2023; 53: 127-35)***

KEY WORDS: Artifacts, Metals, Cone-Beam Computed Tomography, Zinc Phosphate Cement, Resin Cements

Introduction

The use of cone-beam computed tomography (CBCT) technology in clinical dental practice has improved dental diagnostic imaging, allowing the assessment of unique 3-dimensional images beyond what is possible to achieve using conventional 2-dimensional dental images.[1] However, CBCT has limitations related to its cone-beam projection geometry, such as noise, poor soft tissue contrast, and artifacts.[1] An artifact is an undesirable phenomenon that can degrade image quality and compromise the diagnostic process and is defined as an image in the reconstructed data that is not part of the object under investigation.[2,3]

The intensity of beam-hardening artifacts depends on the

This study was financed in part by the Coordenação de Aperfeiçoamento de Pessoal de Nível Superior - Brasil (CAPES) - Finance Code 001.
Received October 14, 2022; Revised January 31, 2023; Accepted February 14, 2023
Published online March 24, 2023
*Correspondence to : Prof. Daniela Pita de Melo
Department of Oral Diagnosis, State University of Paraíba, Rua Baraúnas, 351 - Bairro Universitário Campina Grande, PB, CEP 58429-500, Brazil
Tel) 55-83-3315-3300, E-mail) danipita@gmail.com

Imaging Science in Dentistry · pISSN 2233-7822 eISSN 2233-7830

density of the materials present in the scanned area. Dental materials usually have high density, enabling their identification as radiopaque areas on radiographic images; therefore, they usually increase the intensity of artifacts.[3] The intensity of artifacts produced by high-density materials such as metal posts is directly related to the atomic number of their constituents; higher-atomic-number materials lead to greater degradation of image quality.[2,4-7] Fiber posts are low-density materials that can be used to restore teeth that need intracanal retention; however, metal cores are still used when a large amount of dentin is lost and there is no adequate anchorage for the restoration.[8]

The intensity of high-density material-induced artifacts can be affected by the CBCT scanner,[7,9] imaging acquisition protocol,[6,10] the position of the object within the field of view (FOV), and the presence of an exomass.[11-13] For this reason, the acquisition parameters, detector type, and reconstruction algorithms are important parameters that must be considered while acquiring a scan and evaluating image quality in terms of image noise, contrast resolution, and artifacts.

Considering the influence of these factors on artifact intensity and their expression on CBCT images, the aim of the present study was to assess the intensity of artifacts produced by 2 metal posts, 2 cements, and different exposure parameters in scans using 2 CBCT units. This result would provide useful guidance for operators while selecting acquisition protocols to optimize image quality and minimize patient radiation dose.

Materials and Methods

This *in vitro* experimental study followed the Helsinki Declaration and was approved by the University's Ethics and Research Committee (protocol: 39088714.2.0000.5187).

The sample consisted of 20 single-rooted human teeth (premolars) extracted for therapeutic reasons. All teeth were inspected by transillumination for the absence of root fractures and radiographed on phosphor plates (Digora Optime, Soredex, Tuusula, Finland) to exclude teeth with pulp nodules, internal and/or external root resorption, previous endodontic treatment, root canal multiplicity, root canal obliteration, root fractures, or any other anomaly. The inclusion criteria stated that all teeth should present a maximum root inclination of $\leq 5°$ according to Schneider's method[14] and have similar dimensions.

After cleaning and disinfection protocols, teeth crowns were removed at the cemento-enamel junction, and root canals were standardized using the Reciproc R50 system (VDW, München, Germany) with thermomechanical compression filling, and then prepared to two-thirds of the root length (Peeso Long Drill no. 1 and no. 2, Dentsply/Maillefer, São Paulo, SP, Brazil) for posterior metal post preparation and fitting. The sample was then divided into 2 groups: 10 teeth that received nickel-chromium posts (NiCr group) and 10 teeth that received silver-palladium posts (AgPd group). Subsequently, each group was subdivided equally according to the type of cement used for its restoration: zinc phosphate and Allcem resin cements.

Metal post preparation was performed by the direct technique (standard for metal casting made of Duralay acrylic resin) and the coronary part of the metal post was standardized using a heavy-base condensation silicone matrix (Zetaplus, Zhermack, Badia Polesine, Italy).

The Fit Cast-SB Plus alloy (Talmax Produtos de Prótese Dentária Ltda, Curitiba, PR, Brazil), was used to cast the NiCr post group. For the Ag-Pd post group, the Palad PD-AG alloy (La Croix Dentales, Rio de Janeiro, RJ, Brazil) was used. Periapical radiographs were taken to validate post adaptation. Posteriorly, zinc phosphate cement (S. S. White, Lakewood, NJ, USA) and Allcem resin cement (FGM, Joinville, SC, Brazil) were used for post cementation.

A dentate dry human skull was coated with a 5-mm-thick piece of wax to simulate the interference of soft tissues in the image. Each tooth was coated with a 0.2 mm layer of wax and placed in an empty mandibular right canine socket. The skull was immersed in a foam box filled with water to further simulate soft tissue coverage.[15] Each sample was scanned without the metal post, with the corresponding metal post (NiCr or AgPd), and after cementation with the chosen cement (zinc phosphate or Allcem).

CBCT scans were acquired using 2 scanners: a CS9000 3D (Carestream Dental Rochester, NY, USA), a charge-coupled device (CCD) flat panel, and an i-CAT Cone Beam 3D Imaging System scanner (Imaging Sciences International, Hatfield, PA, USA), an amorphous silicon flat panel with a CsI scintillator.

The CS9000 3D scans were obtained using 2 tube voltage settings (85 kV and 90 kV) and tube currents (6.3 mA and 10 mA). The voxel size and field of view (FOV) were fixed at 0.100 mm and 5 cm × 3.75 cm, respectively. The i-CAT Cone Beam 3D Imaging System scans were obtained with fixed parameters of 120 kV, 5 mA, 0.125 mm voxel size, and 6 cm × 8 cm FOV.

The resulting datasets were exported as Digital Imaging and Communications in Medicine (DICOM) files to be assessed using the corresponding CBCT software: CS9000 3D

Imaging Software (Carestream Dental Rochester, NY, USA) and Xoran CAT v. 3.0.34 software (Xoran Technologies, Ann Arbor, MI, USA). A total of 300 scans were saved, each with a code corresponding to the tooth study conditions and protocol used.

For the subjective analysis of artifacts, 2 experienced oral and maxillofacial radiologists (10 years of experience) assessed all images independently. Prior to all examination sessions, verbal and practical instructions and calibration tests were performed. Adjustments of zoom, brightness, and contrast settings were left to each observer's discretion.

In the subjective analysis, the inter-observer kappa coefficient was 0.400 for hypodense halos, 1.000 for hypodense lines, and 0.700 for hyperdense lines. The intra-observer kappa coefficient for observer 1 was 1.000 for hypodense halos, 0.700 for hypodense lines, and 0.700 for hyperdense lines. For observer 2, the intra-observer kappa coefficient was 0.550 for hypodense halos, 0.625 for hypodense lines, and 0.550 for hyperdense lines.

The scans were subjectively assessed using CS9000 3D Imaging Software (Carestream Dental Rochester, NY, USA) and Xoran CAT v. 3.0.34 software (Xoran Technologies, Ann Arbor, MI), displayed on a 24-inch Dell Ultra Sharp Color Monitor (Dell Inc, Austin, TX, USA) in a quiet, dimly lit room. A daily number of 15 volumes was suggested for evaluation with a minimum interval of 24 hours, but each evaluator could choose his or her individual limit as long as it did not exceed 50 volumes per day.

The amount of image artifacts was scored as absence (0), moderate presence (1), or high presence (2) for hypodense halos (dark bands), hypodense lines (dark lines), and hyperdense lines (bright lines).[4]

For objective artifact quantification, each DICOM file was assessed on the scanner's native software. The axial images were imported into GIMP version 2.8.14 (the GIMP Team, USA, available at: http://www.gimp.org/) and the region corresponding to the whole root area was selected with the free selection tool viewed with a zoom of ×200. The resulting images were set to an 8-bit scale (256 gray levels), saved with a black and a white background in JPEG format, and imported into ImageJ (version 1.48, National Institutes of Health, Bethesda, MD, USA, http://rsb.info.nih.gov/ij/) (Fig. 1).

To remove the area corresponding to the post in the passive or cemented-fit post images, which did not correspond to the artifact images, an overlap was made between the images of the empty tooth and the restored tooth. This step was performed in 3 axial images (cervical, middle and apical core) for each tooth using the ImageJ software to acquire a final image of each axial slice.

For image processing, each axial image of an empty tooth was duplicated, and the threshold tool was applied to convert it to a binary image (0 - root canal and background and 255 - dentin). To enable this process, the values were normalized to a scale where the post and background corresponded to 0 and the dentin to 1. Image subtraction was then performed using the multiplication tool in the program by subtracting the binary that had the empty conduit and dentin from the image with the post and dentin. As a result, the portion of the image corresponding to the post was excluded from the final image (Fig. 2).

When analyzing the dentin area, the threshold tool was used to determine the hypodense and hyperdense artifact areas. In an 8-bit image, with 256 gray levels, the range of hypodense and hyperdense artifacts was determined, and the remaining tooth (non-affected tooth) was the complementary range (Fig. 3). The percentages of these areas were then calculated. When a hypodense artifact was very intense, it was

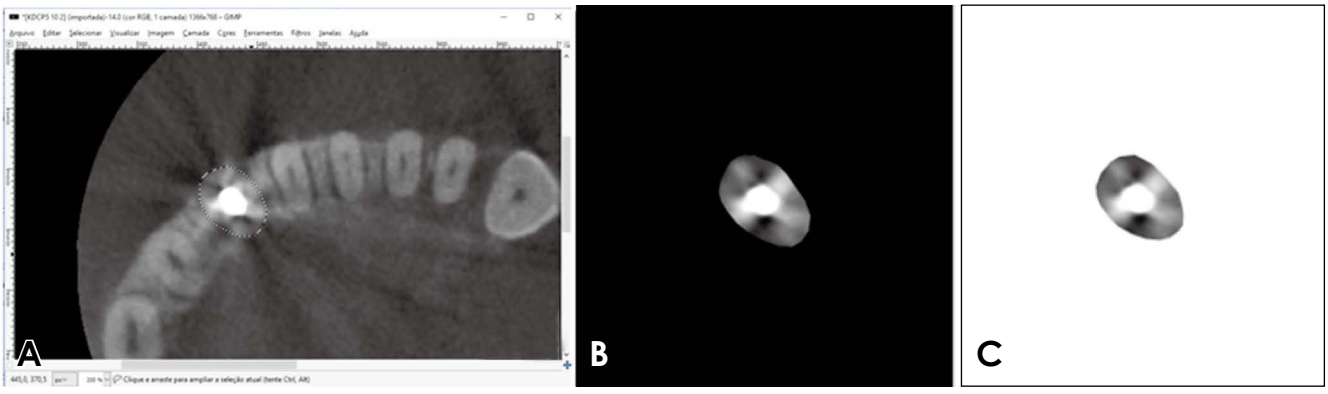

Fig. 1. A. Root area selection using the GIMP program. B. Selected area of the root with a black background. C. Selected area of the root with a white background.

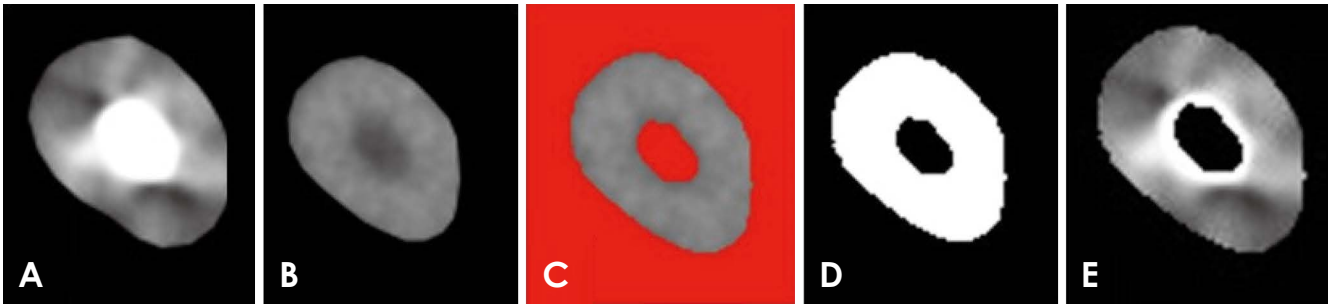

Fig. 2. Image processing for nucleus removal. A. Image of the restored tooth. B. Image of the unrestored tooth. C. Duplicate image of the empty tooth with threshold tool. D. binary image of the empty tooth. E. subtracted image of the restored tooth.

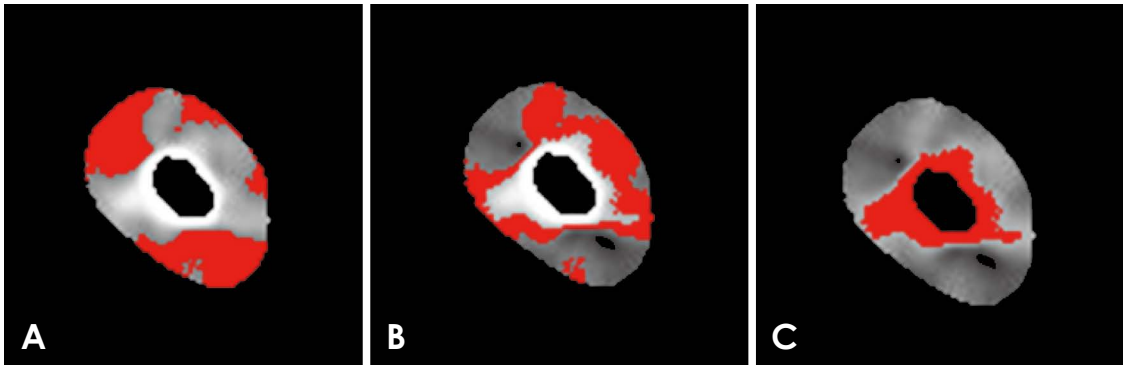

Fig. 3. Selection of the area corresponding to hypodense and hyperdense artifacts with the threshold tool. A. Hypodense artifact. B. Non-affected area of the tooth. C. Hyperdense artifact.

impossible to select it in a black background, because the region had the same pixel value as the image background and the core region. In those cases, a white background image was used to assess the image artifact.

All analyses were performed using SPSS for Windows version 25.0 (IBM Corp., Armonk, NY, USA) with a significance level of 5%. Data were analyzed using descriptive and inferential statistics.

For the subjective analyses, hypodense halos, hypodense lines, and hyperdense lines were the dependent variables. These variables were scored according to the amount of artifacts as absence (0), moderate presence (1), or high presence (2). These ratings were statistically treated as continuous variables, where higher values indicate a higher amount of artifacts. For the objective analyses, the percentage of hypodense artifacts, percentage of tooth area, and percentage of hyperdense artifacts were the dependent variables. The variables were initially descriptively characterized using measures of central tendency, dispersion, and position, and the normality of their distribution was checked using the Kolmogorov-Smirnov test. The variables showed a non-normal distribution; thus, non-parametric tests were used.

The Mann-Whitney test was used to compare the artifacts between the alloys and between the cements. The Wilcoxon test was used to compare artifacts between exposure parameters and between the 2 devices.

Results

Subjective assessment of artifacts

AgPd post scans were subjectively assessed as presenting a higher intensity of hypodense lines ($P<0.05$) and hyperdense lines ($P<0.05$) than NiCr post scans for both studied CBCT scanners and a higher intensity of hypodense halos ($P<0.05$) on the i-CAT scanner than on the CS9000 3D device. No statistically significant differences were found in the intensity of artifacts between the assessed cements for both scanners (Table 1).

Significantly higher intensities of hypodense halos, hypodense lines, and hyperdense lines were observed in scans taken at 10 mA than in those taken at 6.3 mA. Regarding kilovoltage, the 85 kV scans showed a higher intensity of hypodense halo artifacts than scans obtained at 90 kV (Table 2).

Table 1. Statistical comparison of subjective assessments of artifact intensity for metal alloys and endodontic cements using i-CAT and CS9000 3D scanners

		Alloy	Mean	Cement	Mean
i-CAT	Hypodense halos	NiCr	1.03 ± 0.76	Zinc phosphate	1.12 ± 0.78
		AgPd	1.19 ± 0.81*	Resin cement	1.09 ± 0.76
	Hypodense lines	NiCr	1.03 ± 0.72	Zinc phosphate	1.26 ± 0.83
		AgPd	1.49 ± 0.86*	Resin cement	1.26 ± 0.83
	Hyperdense lines	NiCr	0.98 ± 0.70	Zinc phosphate	1.23 ± 0.82
		AgPd	1.49 ± 0.87*	Resin cement	1.24 ± 0.83
CS9000 3D	Hypodense halos	NiCr	1.01 ± 0.79	Zinc phosphate	1.05 ± 0.81
		AgPd	1.10 ± 0.84	Resin cement	1.06 ± 0.82
	Hypodense lines	NiCr	1.12 ± 0.84	Zinc phosphate	1.26 ± 0.88
		AgPd	1.36 ± 0.90*	Resin cement	1.22 ± 0.88
	Hyperdense lines	NiCr	1.13 ± 0.85	Zinc phosphate	1.23 ± 0.89
		AgPd	1.35 ± 0.91*	Resin cement	1.25 ± 0.89

*: $P < 0.05$ by the Mann-Whitney test

Table 2. Statistical comparison of subject artifact intensity according to different exposure parameters for the CS9000 3D unit

	mA	Mean	kV	Mean
Hypodense halos	6.3	0.97 ± 0.80	85	1.03 ± 0.83*
	10	1.01 ± 0.82*	90	0.97 ± 0.80
Hypodense lines	6.3	1.15 ± 0.88	85	1.15 ± 0.88
	10	1.27 ± 0.91*	90	1.15 ± 0.88
Hyperdense lines	6.3	1.13 ± 0.88	85	1.17 ± 0.90
	10	1.22 ± 0.91*	90	1.13 ± 0.88

*: $P < 0.05$ by the Wilcoxon test

Table 3. Subjective comparison of artifact intensity between scans acquired with the i-CAT and CS9000 3D scanners (90 kV, 10 mA)

	Scanner	Mean
Hypodense halos	i-CAT	1.48 ± 0.5
	CS9000 3D	1.51 ± 0.5
Hypodense lines	i-CAT	1.67 ± 0.47
	CS9000 3D	1.89 ± 0.31*
Hyperdense lines	i-CAT	1.62 ± 0.48
	CS9000 3D	1.83 ± 0.38*

*: $P < 0.05$ by the Wilcoxon test

The scans obtained with the CS9000 3D showed higher inten-sity of hypodense lines and hyperdense lines ($P < 0.05$) when compared to the scans obtained with the i-CAT scanner. No statistically significant differences between the CBCT scanners regarding the presence of hypodense halos (Table 3).

Objective analysis of artifacts

AgPd post scans showed higher percentage of hypodense (27.0% and 33.2%) and hyperdense (25.5% and 23.3%) artifacts than NiCr posts for both assessed scanners ($P < 0.05$) (Table 4).

No statistically significant differences were observed in the percentage of artifacts between cements for both scanners ($P > 0.05$), except that a higher percentage of artifacts was observed for the posts cemented with zinc phosphate using the CS9000 3D (21.7%) ($P < 0.05$) (Table 4).

A higher percentage of hyperdense artifacts was found in scans obtained with 10 mA (22.1%) than in those obtained with 6.3 mA (20.3%) ($P < 0.05$). Regarding kilovoltage, a higher percentage of hypodense artifacts was observed in images obtained with 85 kV (35.7%) and a higher percentage of hyperdense artifacts was noted in images obtained with 90 kV (21.3%) ($P < 0.05$) (Table 5).

Scans obtained with the CS9000 3D scanner showed higher percentages of hypodense (29%) and hyperdense (22.2%) artifacts ($P < 0.05$) than those obtained with the i-CAT scanner (26.5% and 19.8%, respectively) (Table 6).

Discussion

In recent years, several studies have focused on assessing the possible variables that may influence the expression of artifacts on CBCT scans, aiming to better understand how to

Table 4. Objective comparison of artifact intensity for metal alloys and endodontic cements using the i-CAT and CS9000 3D scanners

		Alloy	Mean	Cement	Mean
i-CAT	% of hypodense artifacts	NiCr	25.9 ± 5.3	Zinc phosphate	26.2 ± 4.8
		AgPd	27.0 ± 4.3*	Resin cement	26.7 ± 4.9
	% of non-affected tooth area in the image	NiCr	59.9 ± 7.7*	Zinc phosphate	53.8 ± 11.3
		AgPd	47.4 ± 9.3	Resin cement	53.4 ± 9.8
	% of hyperdense artifacts	NiCr	14.1 ± 4.3	Zinc phosphate	19.9 ± 8.9
		AgPd	25.5 ± 6.9*	Resin cement	19.7 ± 7.1
CS9000 3D	% of hypodense artifacts	NiCr	32.0 ± 8.6	Zinc phosphate	32.6 ± 8.5
		AgPd	33.2 ± 8.7*	Resin cement	32.6 ± 8.8
	% of non-affected tooth area in the image	NiCr	49.0 ± 9.7*	Zinc phosphate	45.7 ± 10.6
		AgPd	43.5 ± 10.5	Resin cement	46.8 ± 10.3
	% of hyperdense artifacts	NiCr	18.9 ± 4.9	Zinc phosphate	21.7 ± 6.6*
		AgPd	23.3 ± 7.0*	Resin cement	20.6 ± 6.3

*: $P < 0.05$ by the Mann-Whitney test

Table 5. Objective comparison of artifact intensity according to different parameters for the CS9000 3D scanner

	mA	Mean	kV	Mean
% of hypodense artifacts	6.3	32.0 ± 8.5	85	35.7 ± 9.6*
	10	33.3 ± 8.8	90	28.8 ± 5.1
% of non-affected tooth area in the image	6.3	47.6 ± 10.0*	85	43.3 ± 11.2
	10	44.5 ± 10.7	90	49.8 ± 8.1*
% of hyperdense artifacts	6.3	20.3 ± 6.2	85	20.9 ± 6.4
	10	22.1 ± 6.6*	90	21.3 ± 6.5*

*: $P < 0.05$ by the Wilcoxon test

Table 6. Objective comparison of artifact intensity using the i-CAT and CS9000 3D (90 kV/10 mA) scanners

	Scanner	Mean (SD)
% of hypodense artifacts	i-CAT	26.5 ± 4.8
	CS9000 3D	29.0 ± 5.1*
% of non-affected tooth area in the image	i-CAT	53.6 ± 10.6
	CS9000 3D	48.8 ± 8.1*
% of hyperdense artifacts	i-CAT	19.8 ± 8.1
	CS9000 3D	22.2 ± 6.7*

*: $P < 0.05$ by the Wilcoxon test

assess and improve image quality.[4,7,10] Studies on this topic should always consider and respect the ALADAIP principle ("as low as diagnostically acceptable being indication-oriented and patient-specific"), using the most appropriate acquisition protocol for the specific purpose of the diagnosis.[16]

Metal posts were associated with greater artifact intensity and, therefore, compromised CBCT diagnostic performance in previous studies.[4,5,15,17] Although the use of metal posts has tended to decrease due to fiber posts' aesthetic properties, their similar elastic modulus to dentin, and their tendency to induce favorable root fractures, metal posts are still used when greater retention is needed as a consequence of insufficient remaining dentin. According to Sarkis-Onofre et al.,[18] fiberglass and metal posts presented good and similar clinical performance; therefore, choosing a particular metal alloy that presents lower artifact intensity on CBCT scans can improve the final CBCT image quality.[19,20]

Metal alloys with higher atomic numbers attenuate more X-ray beams and produce higher artifact intensity. In this study, AgPd posts (atomic numbers 47 and 46, respectively) presented higher artifact intensity than nickel-chromium posts (atomic numbers 28 and 24, respectively). In accordance with this study, Panjnoush et al.[19] found that cobalt-chromium alloys led to a higher presence of severe artifacts

than titanium, and Chindasombatjareon et al.[20] found that type IV gold alloys presented the largest artifact areas, followed by cobalt-chromium, titanium, and aluminum alloys.

Codari et al.[7] also reinforced that high-density materials should be considered as being responsible for a variety of artifact manifestations. Amalgam, which is a heterogeneous material composed of high-atomic-number alloys (mercury [Z = 80], silver [Z = 47], tin [Z = 50]), and a low-atomic-number alloy (zinc [Z = 30]) presented higher artifact intensity than CuAl (Z = 39 and 13, respectively) and titanium (Z = 22), which led to substantial volume overestimation during image segmentation. Low-atomic-number alloy dental materials also presented less image noise.[2]

Endodontic post cements should present enough density to be distinguished from the surrounding structures. Root canal materials (obturation and sealing) produced a distinct degree of CBCT image artifacts given their density and composing elements.[21] Few studies have assessed the capability of endodontic cements to induce CBCT artifacts. Freitas-e-Silva et al.[22] found no difference between the evaluated endodontic cements in terms of their influence on vertical root fracture detection. Cavalcanti et al.[23] found that BC Sealer induced significantly more imaging artifacts. In this study, the zinc-phosphate sealer presented higher hyperdense artifact intensity than the resin sealer for the CS9000 3D scanner; however, for the other assessed variables, no statistically significant differences were observed. This result may be explained by the small amount of cement used in the post casting and cementation technique, leaving only a small layer of cement, which may not have been enough to interfere with the overall artifact intensity. Therefore, other studies using different post sealers are needed to assess their effects on artifact intensity.

High-density materials, technical factors, and different CBCT devices should be considered as being responsible for a variety of artifact manifestations.[7] The first step before acquiring a CBCT scan is to set the acquisition and exposure parameters based on the patients' characteristics, indication for the examination, and area of interest. These parameters are paramount for acquiring a high-quality image following the ALADAIP principle.[16,19,20,24]

In this study, higher tube current and lower tube voltage presented higher artifact intensity. The tube current is directly proportional to the amount of X-ray photons exiting the tube and, therefore, to the radiation dose, while tube voltage is related to the tube potential between the cathode and anode and determines the maximum X-ray energy.[25] Low-energy X-ray beams have a greater probability of being absorbed, and increasing the mean energy of the beam causes beam-hardening artifacts. A higher peak kilovoltage reduces beam hardening, while changing the current and exposure time affects noise but not beam hardening.[25]

Lima et al.[26] concluded that low-exposure protocols presented fewer image artifacts in CBCT scans, and Safi et al.[27] also reported that lower mA parameters should be used for the detection of root fractures in teeth restored with intracanal posts. Lower current, higher tube voltage, and a smaller FOV are preferable in order to achieve fewer volumetric distortion artifacts in CBCT scanning.[10] The results of the present study are in accordance with previous studies showing that higher tube voltage settings could reduce the artifact intensity of high-density materials.[3,10,19,28,29]

Different scanners present different FOV sizes, and the FOV size may be associated with a change in the scanning protocol, altering acquisition and exposure parameters.[30] Voxel size may interfere with the detection of vertical root fractures and, in some scanners, is automatically associated with FOV size, with smaller voxels only possible for smaller-FOV protocols.[31]

Previous studies disagreed on the artifact intensity associated with the FOV size. According to Pauwels et al.,[32] large-FOV scanners presented fewer artifacts than small-FOV scanners. However, Khosravifard et al.[33] and Codari et al.[7] reported significantly higher artifact generation by large- and medium-FOV scanners than by small-FOV scanners. In this study, the scanner with the highest FOV presented a lower amount of artifacts than the scanner with the lowest FOV. The inconsistent findings between studies may be related to the different scanners assessed, different acquisition and exposure parameters, and improvements in the performance of modern scanners. However, the use of a large FOV is not justified only for artifact reduction, because when all other parameters are similar, larger-FOV scanners result in higher X-ray doses.[9,33]

In conclusion, high-atomic-number alloys, higher tube current, and lower tube voltage may increase the artifact intensity of CBCT scans. Operators must keep in mind the necessity of correctly choosing the acquisition and exposure parameters based on the ALADAIP principle.

Conflicts of Interest: None

References

1. Scarfe WC, Farman AG. What is cone-beam CT and how does it work? Dent Clin North Am 2008; 52: 707-30.
2. Queiroz PM, Groppo FC, Oliveira ML, Haiter-Neto F, Freitas DQ. Evaluation of the efficacy of a metal artifact reduction algorithm in different cone beam computed tomography scanning

parameters. Oral Surg Oral Med Oral Pathol Oral Radiol 2017; 123: 729-34.
3. Schulze R, Heil U, Gross D, Bruellmann DD, Dranischnikow E, Schwanecke U, Schoemer E. Artefacts in CBCT: a review. Dentomaxillofac Radiol 2011; 40: 265-73.
4. Lira de Farias Freitas AP, Cavalcanti YW, Costa FCM, Peixoto LR, Maia AMA, Rovaris K, et al. Assessment of artefacts produced by metal posts on CBCT images. Int Endod J 2019; 52: 223-36.
5. Fontenele RC, Farias Gomes A, Rosado LPL, Neves FS, Freitas DQ. Mapping the expression of beam hardening artefacts produced by metal posts positioned in different regions of the dental arch. Clin Oral Investig 2021; 25: 571-79.
6. Gaêta-Araujo H, Nascimento EHL, Fontenele RC, Mancini AXM, Freitas DQ, Oliveira-Santos C. Magnitude of beam-hardening artifacts produced by gutta-percha and metal posts on cone-beam computed tomography with varying tube current. Imaging Sci Dent 2020; 50: 1-7.
7. Codari M, de Faria Vasconcelos K, Ferreira Pinheiro Nicolielo L, Haiter Neto F, Jacobs R. Quantitative evaluation of metal artifacts using different CBCT devices, high-density materials and field of views. Clin Oral Implants Res 2017; 28: 1509-14.
8. Gholami F, Kohani P, Aalaei S. Effect of nickel-chromium and non-precious gold color alloy cast posts on fracture resistance of endodontically treated teeth. Iran Endod J 2017; 12: 303-6.
9. Vasconcelos KF, Nicolielo LF, Nascimento MC, Haiter-Neto F, Bóscolo FN, Van Dessel J, et al. Artefact expression associated with several cone-beam computed tomographic machines when imaging root filled teeth. Int Endod J 2015; 48: 994-1000.
10. Celikten B, Jacobs R, deFaria Vasconcelos K, Huang Y, Nicolielo LFP, Orhan K. Assessment of volumetric distortion artifact in filled root canals using different cone-beam computed tomographic devices. J Endod 2017; 43: 1517-21.
11. de Oliveira Pinto MG, Sousa Melo SL, Cavalcanti YW, de Lima ED, Bento PM, de Melo DP. Influence of tooth position within the field of view on the intensity of cone-beam computed tomographic imaging artifacts when assessing teeth restored with various intracanal materials. Imaging Sci Dent 2020; 50: 141-51.
12. Candemil AP, Mangione F, Vasconcelos KF, Oenning AC, Jacobs R, Freitas DQ, et al. Influence of the exomass on the detection of simulated root fracture in cone-beam CT - an ex-vivo study. Dentomaxillofac Radiol 2021; 50: 20200450.
13. Candemil AP, Salmon B, Freitas DQ, Haiter-Neto F, Oliveira ML. Distribution of metal artifacts arising from the exomass in small field-of-view cone beam computed tomography scans. Oral Surg Oral Med Oral Pathol Oral Radiol 2020; 130: 116-25.
14. Schneider SW. A comparison of canal preparations in straight and curved root canals. Oral Surg Oral Med Oral Pathol 1971; 32: 271-5.
15. Pinto MGO, Rabelo KA, Sousa Melo SL, Campos PSF, Oliveira LSAF, Bento PM, et al. Influence of exposure parameters on the detection of simulated root fractures in the presence of various intracanal materials. Int Endod J 2017; 50: 586-94.
16. Oenning AC, Pauwels R, Stratis A, De Faria Vasconcelos K, Tijskens E, De Grauwe A, et al. Halve the dose while maintaining image quality in paediatric cone beam CT. Sci Rep 2019; 9: 5521.
17. Costa FF, Gaia BF, Umetsubo OS, Cavalcanti MG. Detection of horizontal root fracture with small-volume cone-beam computed tomography in the presence and absence of intracanal metallic post. J Endod 2011; 37: 1456-9.
18. Sarkis-Onofre R, Amaral Pinheiro H, Poletto-Neto V, Bergoli CD, Cenci MS, Pereira-Cenci T. Randomized controlled trial comparing glass fiber posts and cast metal posts. J Dent 2020; 96: 103334.
19. Panjnoush M, Kheirandish Y, Kashani PM, Fakhar HB, Younesi F, Mallahi M. Effect of exposure parameters on metal artifacts in cone beam computed tomography. J Dent (Tehran) 2016; 13: 143-50.
20. Chindasombatjaroen J, Kakimoto N, Murakami S, Maeda Y, Furukawa S. Quantitative analysis of metallic artifacts caused by dental metals: comparison of cone-beam and multi-detector row CT scanners. Oral Radiol 2011; 27: 114-20.
21. Decurcio DA, Bueno MR, de Alencar AH, Porto OC, Azevedo BC, Estrela C. Effect of root canal filling materials on dimensions of cone-beam computed tomography images. J Appl Oral Sci 2012; 20: 260-7.
22. Freitas-E-Silva A, Mármora B, Barriviera M, Panzarella FK, Raitz R. CBCT performance and endodontic sealer influence in the diagnosis of vertical root fractures. J Contemp Dent Pract 2019; 20: 552-6.
23. Cavalcanti MGP, Salineiro FC, Barros FM, Barros FBA. Influence of endodontic sealers artifacts in the detection of vertical root fractures. Braz Dent J 2022; 33: 22-30.
24. Katkar R, Steffy DD, Noujeim M, Deahl ST 2nd, Geha H. The effect of milliamperage, number of basis images, and export slice thickness on contrast-to-noise ratio and detection of mandibular canal on cone beam computed tomography scans: an in vitro study. Oral Surg Oral Med Oral Pathol Oral Radiol 2016; 122: 646-53.
25. Pauwels R, Seynaeve L, Henriques JC, de Oliveira-Santos C, Souza PC, Westphalen FH, et al. Optimization of dental CBCT exposures through mAs reduction. Dentomaxillofac Radiol 2015; 44: 20150108.
26. Diniz de Lima E, Lira de Farias Freitas AP, Mariz Suassuna FC, Sousa Melo SL, Bento PM, Pita de Melo D. Assessment of cone-beam computed tomographic artifacts from different intracanal materials on birooted teeth. J Endod 2019; 45: 209-13.e2.
27. Safi Y, Hosseinpour S, Aziz A, Bamedi M, Malekashtari M, Vasegh Z. Effect of amperage and field of view on detection of vertical root fracture in teeth with intracanal posts. Iran Endod J 2016; 11: 202-7.
28. Esmaeili F, Johari M, Haddadi P, Vatankhah M. Beam hardening artifacts: comparison between two cone beam computed tomography scanners. J Dent Res Dent Clin Dent Prospects 2012; 6: 49-53.
29. Freitas DQ, Fontenele RC, Nascimento EHL, Vasconcelos TV, Noujeim M. Influence of acquisition parameters on the magnitude of cone beam computed tomography artifacts. Dentomaxillofac Radiol 2018; 47: 20180151.
30. de Oliveira Pinto MG, Melo SLS, Suassuna FCM, Marinho LE, Leite JBDS, Batista AUD, et al. Influence of size of field of view (FOV), position within the FOV, and scanning mode on the detection of root fracture and observer's perception of artifacts in CBCT images. Dentomaxillofac Radiol 2021; 50: 20200563.

31. Yamamoto-Silva FP, de Oliveira Siqueira CF, Silva MAGS, Fonseca RB, Santos AA, Estrela C, et al. Influence of voxel size on cone-beam computed tomography-based detection of vertical root fractures in the presence of intracanal metallic posts. Imaging Sci Dent 2018; 48: 177-84.
32. Pauwels R, Stamatakis H, Bosmans H, Bogaerts R, Jacobs R, Horner K, et al. Quantification of metal artifacts on cone beam computed tomography images. Clin Oral Implants Res 2013; 100: 94-9.
33. Khosravifard A, Saberi BV, Khosravifard N, Motallebi S, Kajan ZD, Ghaffari ME. Application of an auto-edge counting method for quantification of metal artifacts in CBCT images: a multivariate analysis of object position, field of view size, tube voltage, and metal artifact reduction algorithm. Oral Surg Oral Med Oral Pathol Oral Radiol 2021; 132: 735-43.